AADE-22-FTCE-006

Non-Newtonian Flow in Clogged Non-Circular Piping Conduits

Jamie A. Chin, Stratamagnetic Software, LLC, Oklahoma City, Oklahoma

Abstract

Nonlinear fluid flow models in circular conduits, long available for drilling and offshore applications, have supported accurate and effective operational planning for decades. Closed-form analytical solutions for Newtonian, Power Law, Bingham Plastic and Herschel-Bulkley rheologies have demonstrated their utility in numerous field endeavors and have proven to be indispensable in day-to-day calculations.

A limitation in all available models is the restriction to circular cross-sections. Non-circular area effects are approximately handled by changing pipe radius, but the flow rate and pressure gradient relationship *does* depend *strongly* on clog geometry. For example, drilling debris, subsea wax and hydrates, depending on the physical process, may distribute at the bottoms, sides and tops of flow conduits with resulting cross-sectional geometries defying simple or elegant description. Thus, engineers are left without predictive methods that support operational decisions, except for costly, time-consuming and labor-intensive empirical lab studies.

In our approach, the locus of the clog and fluid interface, defined by user-selected points, is used to develop smooth boundary-conforming curvilinear grids honoring the details of any general clog. Stair-step, block-like and "lumpy" approximations are not used. The momentum equations for the above rheological models are rewritten in these coordinates, and numerically solved for axial velocity with zero slip velocity constraints for both pressure and flow rate formulations. The rapid, stable model requires just seconds of desk time on Windows computers, and color displays for velocity, apparent viscosity, stress and strain are automatically integrated. Numerical details are offered and different clog geometries are considered, demonstrating the versatility of the new approach. Apparent viscosity, shear rates and shear stresses are calculated from these velocity distributions.

In this paper, we stress the important role of viscous shear stress in debris and clog removal – detailed physical discussions and examples are given.

Introduction

Clogged pipelines are as old as civilization itself and cover broad applications in modern petroleum, mechanical and civil engineering. There are presently no ideal engineering models that support general diagnostics or mathematical analysis. The examples in Figure 1 point to wide ranges of physical parameters such as diameter, fluid rheology, debris type and general deposition geometry that must be considered. Annual maintenance expenses worldwide are high and address pigging operations, periodic cleaning, blockage detection and removal, and both major repairs and upgrades. Clogs and debris can be removed by increasing surface viscous shear stress, for example, by increasing volume flow rate or by introducing additives that alter the fluid rheology. An accurate and versatile model supporting such needs is required and we summarize the approach and results for our new model here.

Figure 1. Clogged pipelines in petroleum, mechanical and civil engineering operations – broad ranges in diameters, fluid rheology, debris type and general deposition geometry.

Methodology and Approach

Classical Mathematical Solutions

Pipe flow solutions are among the first developed by fluid-dynamicists in the nineteenth century because of their simple mathematical character. Assumptions include circular cross-sections, as in Figure 2, together with requirements for smooth surfaces, laminar behavior, incompressibility, minimal inlet effects, rigid boundaries, steady conditions and zero rotation. Available solutions apply to Newtonian, Power Law, Bingham Plastic, Herschel-Bulkley and Ellis rheologies, among others used in chemical engineering practice.

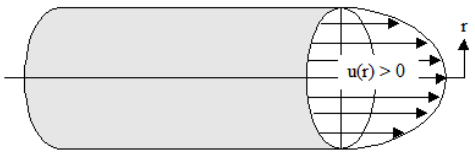

Figure 2. Axisymmetric pipe flow assumption.

Newtonian flow solution. The earliest solution to the Navier-Stokes equations applies only to Newtonian fluids like air, water and certain oils. There are the Hagen-Poiseuille formulas below, applicable to Figure 2 where the axial velocity $u(r) > 0$ depends on the radial coordinate $r > 0$. With this convention, the "shear rate" $du/dr < 0$ is negative, that is, $u(r)$ decreases as r increases. The notation $d\gamma/dt = - du/dr > 0$ is often used. If the viscous shear stress τ and the shear rate are linearly related by $\tau = - \mu\, du/dr > 0$, where μ is a constant viscosity, then two simple relationships follow. Let $\Delta p > 0$ be the (positive) pressure drop over a pipe of length L, and R be the inner radius of the pipe. Then, the radial velocity distribution satisfies $u(r) = [\Delta p/(4\mu L)] (R^2 - r^2) > 0$. Note that u is constrained by a "no-slip" velocity condition at $r = R$. If the product of "u(r)" and the infinitesimal ring area "$2\pi r\, dr$" is integrated over (0,R), we obtain the volumetric flow rate expressed by $Q = \pi R^4 \Delta p/(8\mu L) > 0$. Observe that the viscous stress (and its wall value τ_w) can be calculated from the above, leading to $\tau(r) = r\, \Delta p/2L > 0$ and $\tau_w = R\, \Delta p/2L > 0$. Viscous wall shear stresses are important in pipe operations because higher levels (together with dynamic erosion) act to retard clogging due to surface adhesion. On the other hand, pressures are important in the sense that they may help to dislodge larger pipeline blockages.

Bingham Plastic pipe flow. The limitations in the Hagen-Poiseuille flow solution were recognized early on. Bingham Plastics satisfy a slightly modified constitutive relationship, usually written in the form $\tau = \tau_0 - \mu\, du/dr$ where τ_0 represents the yield stress of the fluid. In other words, fluid motion will not initiate until stresses exceed the yield threshold; in a moving fluid, a "plug flow" moving as a solid body is always found below a "plug radius" defined by $R_p = 2\tau_0 L/\Delta p$.

Thus the "if-then" nature of the model renders it nonlinear, despite the (misleading) linear appearance of the stress-strain relationship. Fortunately, simple solutions are known, where $u(r) = (1/\mu)\, [\{\Delta p/(4L)\} (R^2 - r^2) - \tau_0 (R - r)]$, $R_p \le r \le R$, and $u(r) = (1/\mu)\, [\{\Delta p/(4L)\} (R^2 - R_p^2) - \tau_0 (R - R_p)]$, $0 \le r \le R_p$ with $Q/(\pi R^3) = [\tau_w/(4\mu)]\, [1 - 4/3 (\tau_0/\tau_w) + 1/3\, (\tau_0/\tau_w)^4]$.

Power Law fluid pipe flow. These fluids, without yield stress, satisfy the Power Law $\tau = K(-du/dr)^n$ model where n and K are constants. The corresponding axial velocity is found as $u(r) = (\Delta p/2KL)^{1/n} [n/(n+1)]\, (R^{(n+1)/n} - r^{(n+1)/n})$. Then the volume flow rate is $Q/(\pi R^3) = [R\Delta p/(2KL)]^{1/n} n/(3n+1)$.

Herschel-Bulkley pipe flow. This combines Power Law with yield stress characteristics, $\tau = \tau_0 + K(-du/dr)^n$, so that

$$u(r) = K^{-1/n} (\Delta p/2L)^{-1} \{n/(n+1)\} \times [(R\Delta p/2L - \tau_0)^{(n+1)/n} - (r\Delta p/2L - \tau_0)^{(n+1)/n}],\ R_p \le r \le R$$

$$u(r) = K^{-1/n} (\Delta p/2L)^{-1} \{n/(n+1)\} \times [(R\Delta p/2L - \tau_0)^{(n+1)/n} - (R_p\, \Delta p/2L - \tau_0)^{(n+1)/n}],\ 0 \le r \le R_p$$

$$Q/(\pi R^3) = K^{-1/n} (R\Delta p/2L)^{-3} (R\Delta p/2L - \tau_0)^{(n+1)/n} \times [(R\Delta p/2L - \tau_0)^2\, n/(3n+1) + 2\tau_0 (R\Delta p/2L - \tau_0)\, n/(2n+1) + \tau_0^2\, n/(n+1)]$$

Ellis fluid pipe flow. Finally, Ellis fluids satisfy a more complicated zero yield stress constitutive relationship with $\tau = - du/dr/(A + B\, \tau^{\alpha-1})$. The velocity and flow rate solutions are $u(r) = A\, \Delta p\, (R^2 - r^2)/(4L) + B(\Delta p/2L)^{\alpha}\, (R^{\alpha+1} - r^{\alpha+1})/(\alpha + 1)$ and a volume integral given as $Q/(\pi R^3) = A\tau_w/4 + B\tau_w^{\alpha}/(\alpha+3) = A(R\Delta p/2L)/4 + B(R\Delta p/2L)^{\alpha}/(\alpha+3)$. As noted earlier, other rheological models appear in the literature. Typical qualitative features of the main models for velocity appear in Figure 3.

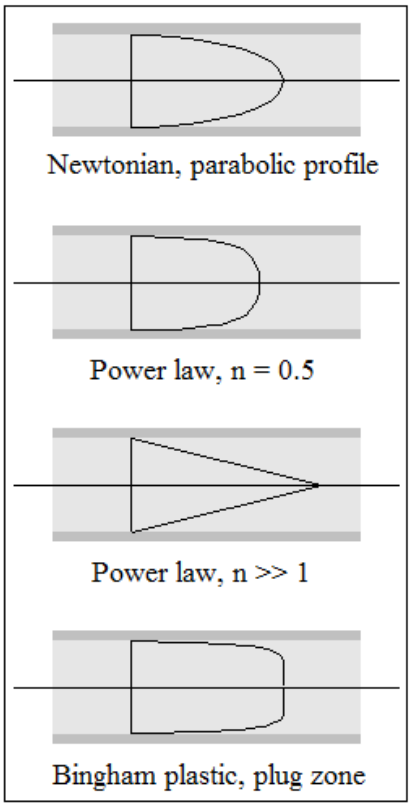

Figure 3. Typical Newtonian and non-Newtonian *axisymmetric/concentric* axial velocity profiles.

The above solutions are important for several reasons. They all give the dependence of velocity, volume flow rate and pressure drop on the basic geometric and rheological parameters, and provide engineers with means to provide "back of the envelope" estimates in field or office work. Note that the dependencies are more complicated than those in the simplest Hagen-Poiseuille relationships. The results also support nonlinear "Q versus Δp" graphical plots that are important operationally and in purchase decisions. However, they are restricted to purely circular cross-sections, thus limiting their applicability to somewhat unrealistic ideal flows that are unlike those shown in Figure 1, where the dependence on geometry is general. Hence, it has proven impossible to develop useful models that support basic "pressure versus rate" needs as well as important surface viscous stress estimates required for pigging and maintenance operations. This overall problem is addressed in the present paper where we introduce a new approach to pipe flow modeling.

Motivation for Non-Circular Cross-Sectional Grids

Axisymmetric math models assuming circular cross-sections permit closed-form mathematical models but are clearly not suitable for clog analysis and remediation applications because of azimuthally-dependent depositional processes. Thus, "boundary-conforming" or curvilinear coordinate grid systems are needed, understanding now that geometric complexities will preclude the possibility of analytical solutions. Three grid strategies are immediately apparent from Figure 4, but are sub-optimal. It is important to emphasize the differences between these conventional grid options and our approach. In (a), low grid densities provide poor physical resolution, worsened by the inability to resolve curvature-related details at boundaries. These are usually resolved by interpolation, which introduces numerical noise. In (b), finer local grids are used to overcome the problems in (a), but the meshes are inefficiently employed. For instance, fine grids near the duct center are not needed; at boundaries, noise is again found that depend on grid size and aspect ratio.

The boundary-conforming polar-like grid in (c) does not introduce interpolation noise, and will accommodate geometric complexities with smaller numbers of grids. This is acceptable. However, for general shapes, it is not clear where the "origin" or "center" is and what boundary conditions might apply at that location. This renders mathematical flow formulations extremely difficult if not impossible to solve. Ideally, a robust formulation would *not* need a center and proceed as if the duct behaved like a square or a rectangular. Further, if numerical outputs for shear stresses could coincide with top, bottom and side locations, analyses for clog removal and pigging operations would be direct and straightforward.

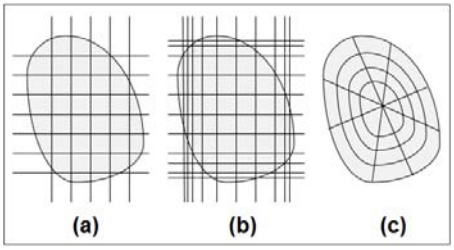

Figure 4. Conventional gridding options.

Alternatively, it might be more interesting to use "rectangle-based" mesh systems for "circle-like" cross-sections. One would solve for the velocity field (subject to no-slip conditions) first, and then post-process it to produce shear rate, shear stress and apparent viscosity distributions. Solutions based on such grids would yield results like those for shear rate shown in Figure 5 directly. Carefully note the appearance of background superposed quadrilaterals – these contrast with the "pizza slices" evident from Figure 4c. For the perfect circular duct shown, the left plot for shear rate $\partial U/\partial x$ (where "x" is the vertical coordinate) provides immediately useful information for top and bottom clog erosion. The obvious red zones easily indicate the magnitude of the relevant high viscous stresses needed for debris removal at the top and bottom. Similarly, the right plot for $\partial U/\partial y$ (where "y" is the horizontal coordinate) supports applications where debris cling to piping sidewalls.

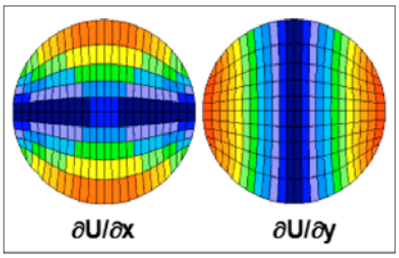

Figure 5. "Rectangle-based" grids (ideal for clog analyses and remediation since viscous stresses are available at "x" and "y" top, bottom and left-right sidewall locations).

Again, the mesh inherent to Figure 5, shown with superposed grid lines, is "rectangular" in nature and ideal for clog analyses since clogs typically form at top, bottom and sidewall pipe locations – precisely where viscous stresses are now easily available for cleaning estimates. Now, Figure 5 was originally developed for Newtonian flows, where shear rates are direct indicators of shear stress. But just how are the underlying coordinate systems defined and how are the relevant non-Newtonian momentum fluid equations integrated into this framework? Before we address the solution process, we explain *why* viscous shear stresses are important to debris removal – this physical principle motivated our search for means to calculate surface stresses in complicated geometries.

Annular Flow Cuttings Transport Removal

The *pipe flow* work in this paper is closely related to prior *annular flow* modeling efforts (Chin 2012). The earlier work addressed cuttings debris removal in deviated and horizontal wells, a problem confronting the industry described in detailed laboratory experiments (Becker et al. 1989). The experimenters were not able to correlate cuttings transport efficiency with any obvious drilling parameters. However, it later turned out that successful cause and effect relationships were possible with the top-of-bed viscous stress taken as the correlation parameter. In retrospect, stresses clearly remove cuttings the same way erasers remove pencil smudges. Our algorithm facilitated viscous stress calculations in the highly eccentric annular spaces found in horizontal drilling.

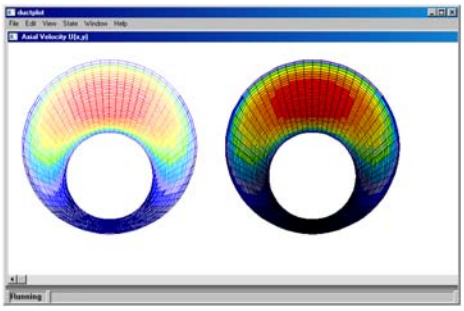

Figure 6a. Annular flow planar velocity plot.

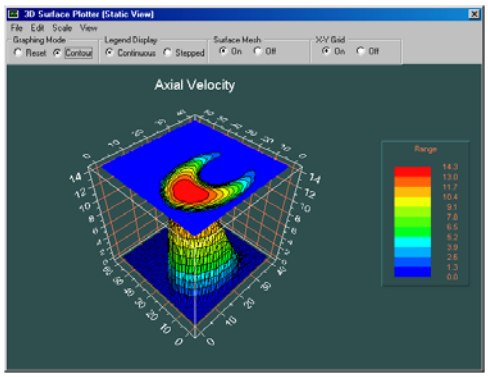

Figure 6b. Annular flow three-dimensional velocity plot.

The annular flow model developed at the time assumed the general "doubly-connected" contour at the top of Figure 7. Normally, solutions are solved using approaches similar to that in Figure 4 – together with all their limitations. Instead, the annular region was "mapped" or transformed to the "singly-connected" (fictitious) duct problem at the bottom of Figure 7. When this is done, simple, easily programmed algorithms are possible. For instance, the simple double-nested Fortran loop for "NMAX" integrations below, executed in the index space `1 < I < IMAX` and `1 < J < JMAX` is all that is required to produce converged axial velocities `U(I,J)`.

```
      DO 200  N = 1, NMAX
      DO 100  I = 1, IMAX
      DO 100  J = 1, JMAX
      U(I,J) = . . .
  100 CONTINUE
  200 CONTINUE
```

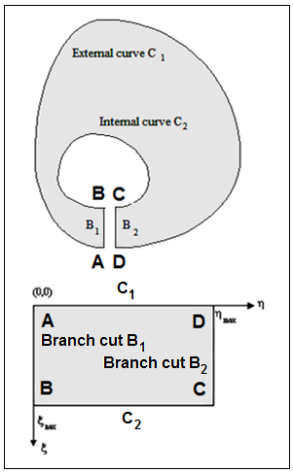

Figure 7. Mapping physical to computational plane.

The mapping transformation requires the introduction of the two "branch cuts" B_1 and B_2 at the top of Figure 7 which convert the annulus to simple duct form. The fictitious cuts, which are mathematical artifacts, require only that `U(I,J)` and its derivatives remain continuous from one cut to the other. In other words, for the *artificial* duct, sudden physical changes are disallowed.

We now turn our attention to Figure 8, which shows two *physically realizable* ducts. There are no mathematical differences between artificial and physically realizable duct formulations except that (1) the former satisfy "smoothness" conditions at B_1 and B_2, while (2) the latter satisfy actual physical "no slip" velocity conditions. Both ducts in Figure 8 are regarded as four-sided, with sides AB, BC, CD and DA (and corners) arbitrarily chosen by the user.

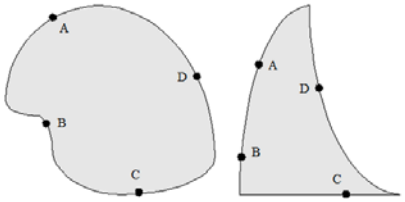

Figure 8. General *four corner* (y,x) cross-sections.

Now we overlay the duct of interest on graph paper, and select or "pencil in" points (y_1,x_1), (y_2,x_2), (y_3,x_3) and so on, along the entire closed physical curve. These y and x values are assigned to the four edges shown, with AB corresponding to the left of the rectangle in Figure 7, AD the top, DC the far right, and CB the bottom. The rectangle is defined in (ξ,η) space, so that AB lies along $\eta = 0$ and $0 < \xi < \xi_{max}$ and CD along $\eta = \eta_{max}$ and $0 < \xi < \xi_{max}$ (there are equal numbers of (y,x) points on AB and CD). Similar considerations apply to BC and DA. With (y,x) known along the boundary curve in the (ξ,η) plane, a coupled nonlinear boundary value problem for $(\,)\,x_{\xi\xi} + (\,)\,x_{\xi\eta} + (\,)\,x_{\eta\eta} = 0$, $(\,)\,y_{\xi\xi} + (\,)\,y_{\xi\eta} + (\,)\,y_{\eta\eta} = 0$ is solved where the $(\,)$ are known functions of x_ξ, x_η, y_ξ and y_η. Once the solution for $x(\xi,\eta)$ and $y(\xi,\eta)$ is available, the governing equation for the velocity u(y,x) for any rheological model is re-expressed in (ξ,η) coordinates and solved subject to no-slip conditions along all solid pipe boundaries. For the curvilinear grids used in this paper, mesh and velocity solutions can be obtained in five seconds on Windows i5 machines. Point relaxation methods were used to solve all partial differential equations. For details, readers are referred to earlier papers due to (Thompson 1984) and (Thompson et al. 1985) and the refinements developed in (Chin 2012).

Our duct flow software development, building on existing annular flow work, actually required much less effort. With the "artificial to physical" duct modification introduced earlier, the eccentric annular flow simulator was converted to one for general duct cross-sections by modifying only five lines of Fortran source code. Of course, this simplification was only possible with the "out of box" realization that physical ducts and, in fact, any ducts with closed contours, can be mapped into rectangular spaces – including triangular, polygonal and distorted-oval shapes. We emphasize that the successful *physical* correlation between cuttings debris removal in drilling annular spaces and cuttings bed surface viscous stress motivated the present work on clog remediation in non-circular pipes. We are also fortunate that the annular flow algorithm could be converted to solve non-Newtonian flows in ducts having general conduit cross-sections.

We offer a short case study analysis on the role of surface viscous shear stress in debris removal. Extensive flow loop experiments were performed at the University of Tulsa and the annular data is publicly available (Becker et al. 1989). Figure 9 shows remaining cuttings concentrations decreasing as surface viscous stress increases. The black shapes represent data points obtained by actual volume measurements while the straight lines correspond to eccentric annular flow model calculations. The successful correlations shown were obtained at all well deviation angles. We expect this physical principle to remain valid in pipe flows as well. All that was needed at the outset of our work was a computational means to calculate such stresses for arbitrary clog cross-sections. Again, it is important to emphasize the differences between the grid formulations shown in Figures 4a,b,c versus our use of somewhat non-intuitive rectangular systems as in Figure 5 for general duct flows. To reiterate, the velocity formulation applies to Newtonian and non-Newtonian fluids, while shear rates, shear stresses and apparent viscosities are post-processed from converged velocity fields.

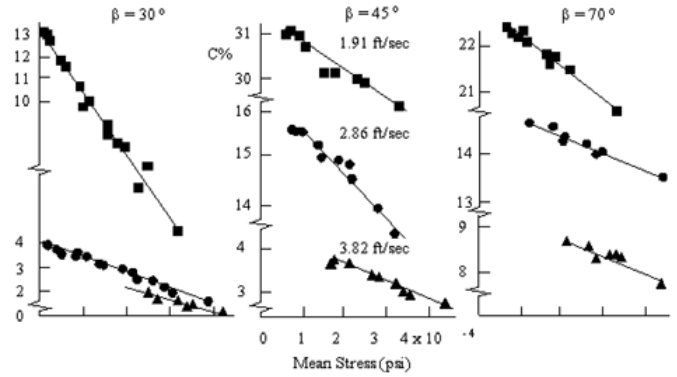

Figure 9. Computed viscous stress cleaning correlations for lab cuttings transport removal at the University of Tulsa.

Computational Results and Detailed Examples

Example 1. Non-Newtonian Power Law Circular Pipe Flow in Rectangle-Like Coordinates.

In this example, we evaluate our use of rectangular coordinate approaches for a Power Law fluid flow in a circular conduit, here comparing solutions with exact azimuthal results obtained analytically. We consider n = 0.9 with k = 17 mPa s^n = 0.000002466 psi s^n for the same pipe radius of 0.59 in (or 1.5 cm) and a volume flow rate of Q = 0.01585 gpm (or 1 cc/s). The coordinates in Figure 5 were again used in the simulations, since in the Newtonian calibration run, errors less than 1% were found. As shown in Figure 10-2a, the exact pressure gradient is found to be 0.00004287 psi/ft. When our finite difference model is run with the built-in mesh generator, the pressure gradient 0.00003738 psi/ft is obtained with the flow rate 0.01593 gpm. The difference in flow rate is about 0.5% while that for pressure gradient is near 14%. In practical engineering calculations, we would adjust the mesh until pressure gradients, flow rates and wall stresses closely agree – only then would we use the mesh to study the implications of different clog geometries. However, as the purpose of this work is to understand mesh effects and the basic feasibility of the curvilinear grid approach, we defer such modifications to future studies. Results are shown in Figure 10-2b.

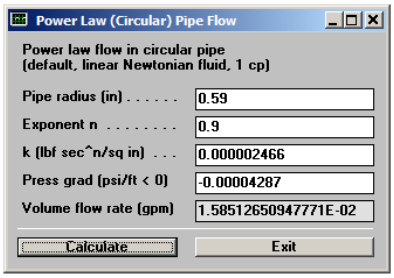

Figure 10-2a. Exact Power Law pipe flow solver "app."

```
No-slip velocity conditions everywhere.
Geometry input from DUCTFILE.DAT file.

POWER LAW FLOW OPTION SELECTED.

Power law fluid assumed, with exponent "n" equal
to .9000E+00 and consistency factor of .2466E-05
lbf sec^n/sq in.

Target flow rate of .1585E-01 gal/min specified.

O  Axial pressure gradient of .3738E-04 psi/ft
   yields volume flow rate of .1593E-01 gal/min.

   Pressure gradient found iteratively, .3738E-04 psi/ft,
   yielding .1593E-01 gal/min vs target .1585E-01 gal/min.

   Total, volume flow rate:  .1593E-01 gal /min
   Cross - sectional  area:  .1094E+01 sqr inch
   Kinetic energy, density:  .2158E-02 in^4/s^2

   TABULATION OF CALCULATED AVERAGE QUANTITIES:
   Area weighted means for absolute value taken
   over entire pipe (x,y) cross-sectional area

O  Axial flow velocity  (inches / sec):  .4970E-01
O  Apparent viscosity (lbf sec / sqin):  .2863E-05
O  Viscous stress AppVis x dU/dx (psi):  .4316E-06
O  Viscous stress AppVis x dU/dy (psi):  .5239E-06
O  Dissipation fnctn (lbf/(sec sq in)):  .2475E-06
O  Shear rate dU/dx (Recip sec, 1/sec):  .1564E+00
O  Shear rate dU/dy (Recip sec, 1/sec):  .1890E+00
O  Stokes product Vel x ApVis (lbf/in):  .1486E-06
```

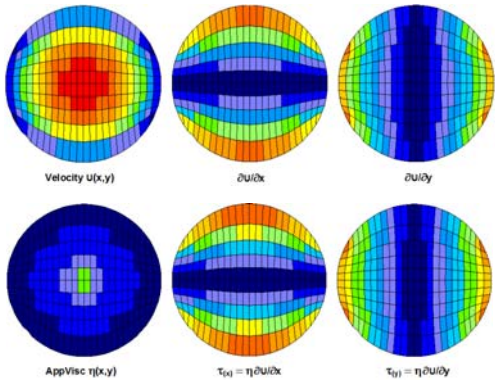

Figure 10-2b. Circle flow properties using (y,x) solver – note the *variable* apparent viscosity field obtained.

It is important to comment on the above display and explain why more plots are given than those in Figure 5. For Newtonian fluids, as given in Figure 5, the assumed viscosity μ is the same constant everywhere, so that shear stress and shear rate color plots, aside from their magnitudes, would be duplicative. Hence, stress plots are omitted. The viscosity (versus x and y) is also not plotted because its value is given and fixed everywhere. The situation is different for non-Newtonian flows. In Figure 10-2b, the "apparent viscosity" is seen to vary with space. Consequently, plots for shear stresses and shear rates will differ qualitatively as well as quantitatively. In the case of yield stress rheologies (like Bingham Plastic and Herschel-Bulkley fluids), the central velocity will be broader and flatter, as in Figure 3. We emphasize that apparent viscosities will differ from one pipe radius or flow rate to another. Laboratory-measured viscosities (taken at an arbitrary fixed shear rate) will be limited in value in actual downhole or pipe flow problems where shear rates and apparent viscosity vary with position.

Example 2. Non-Newtonian velocity fields with large and gradual overhead obstructions.

Self-explanatory velocity results for pipeline flows with large and gradual overhead obstructions are presented below. Red zones indicate maximums within each diagram and will represent different values from case to case. The results shown were assembled from multiple independent runs. Again, it is possible to derive shear rate, viscous shear stress and apparent viscosity from the calculated velocity field, but for brevity, this is deferred to Example 4.

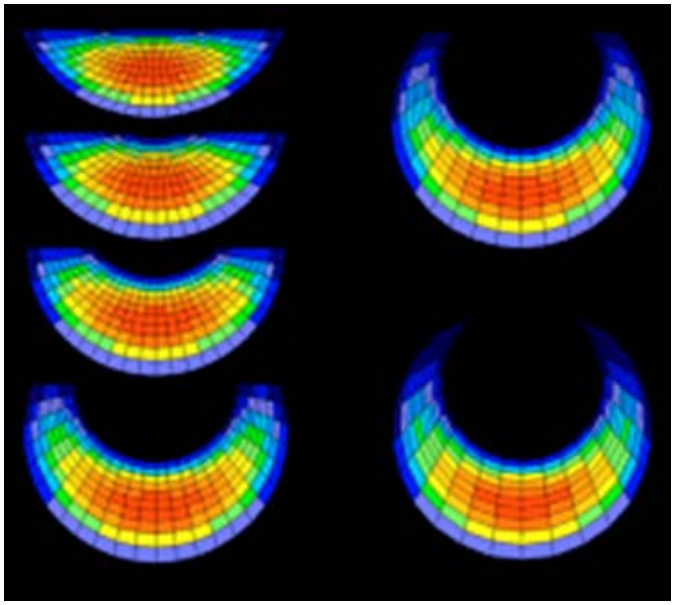

Figure 10-5a. Influence of clog size on velocity field – the same colors in different frames denote different velocities.

Example 3. Non-Newtonian axial velocities encountering sudden and sharp obstacles.

Velocities for flows with sudden and sharp obstacles are offered below. As in Example 2, red zones indicate maximums within each diagram and will represent different values from case to case (the results shown were assembled from multiple independent runs). Again, we can derive shear rate, viscous shear stress and apparent viscosity from the calculated velocity field *and* plot them, but for brevity, this is deferred to the next example.

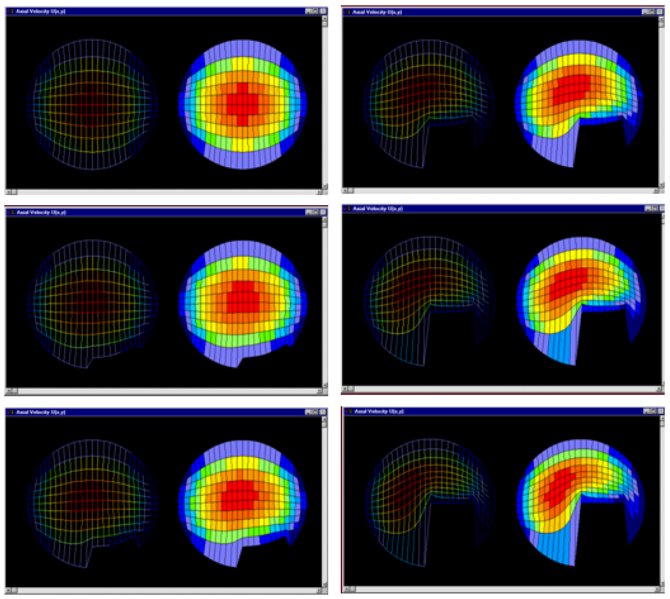

Figure 10-5b. Influence of clog size on velocity field – the same colors in different frames denote different velocities.

Example 4. Non-Newtonian flow in arteries, capillaries and veins.

Flows in arteries, veins and capillaries provide examples of real-world transient clogging motions. Despite the biologically-oriented title in this calculation, we emphasize that such flows *are* legitimate pipe flows nonetheless. Flows in the main aorta are largely Newtonian, while here we focus on those in the smaller arteries, veins and capillaries which are non-Newtonian. The static model developed in our work can be incorporated into dynamic "time lapse" movies that show the clogging process evolving in time. The time lapse sequence below models a complex biological process due to ongoing plaque formation that is countered by a coupled erosion model. The erosion model alters local clog thickness as a function of surface stress and dynamic erosion using a postulated empirical mechanism. This model can be evaluated using laboratory or clinical data. The approach also applies to wax, hydrate or debris deposition in subsea pipelines or general cleaning in surface applications.

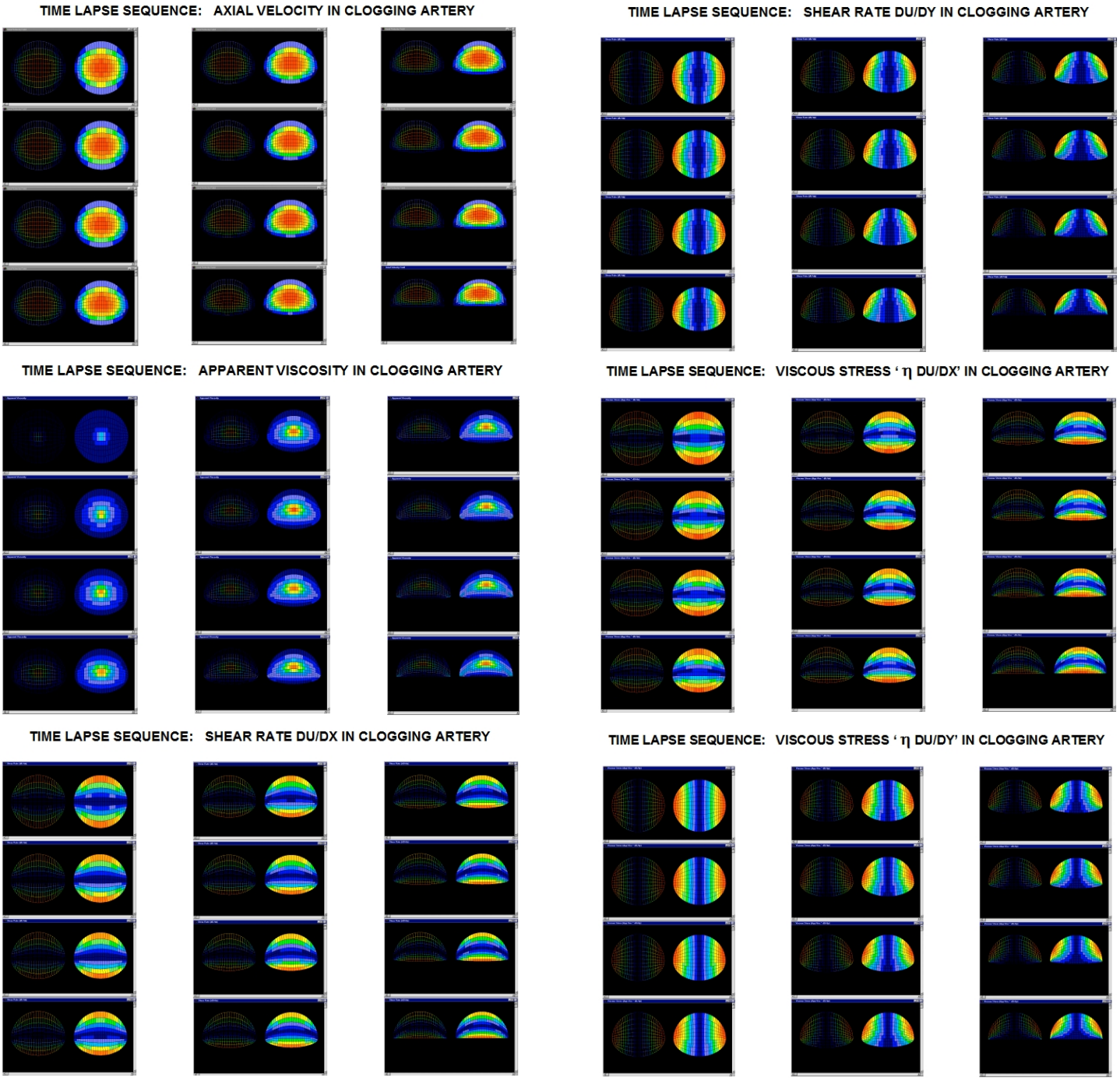

Figure 10-7d. Time lapse movie frames for axial velocity, apparent viscosity, and rectangular x and y shear rates and viscous stresses are shown. The stresses will affect buildup and clog movement in arteries and veins and also in general pipeline problems. Transient area reductions in time are the cumulative effect of a physical build-up mechanism, viscous shearing and dynamic erosion. Note that volume flow rate versus pressure gradient curves are also possible using the methodology.

Example 5. A Software Clog Workflow Plan.

In the simulations below, we assume a radius of 0.25 inch (or a diameter of 0.5 inch), the size of a small feeder pipe where non-Newtonian effects are important. Our objective is to demonstrate the features behind our formulation and methods of validation rather than altering meshes to match data. Altering mesh sizes and distributions is required of all simulators since different grids will yield different solutions – matching data alone does not really validate solution integrity. We consider Newtonian flow in a perfect circle first, followed by Power Law flow in a circle, and then Power Law in a clogged flow.

Simulation No. 1 – Newtonian flow in a perfect circle.

We first consider the Newtonian limit where two exact analytical solutions for volume flow rate are available when pressure gradient is specified. The "1 cp" Newtonian and "0.0000001465 lbf sec^n/in^2" Power Law viscosity specifications are identical. A pressure gradient test value is taken of – 0.0001 psi/ft. The results in Figure 10-8a, using Newtonian and Power Law solutions, consistently show a volume flow rate of 0.02266 gpm (where "gpm" refers to "gallons per minute" – these "app" simulators were originally developed from the analytical solutions cited previously).

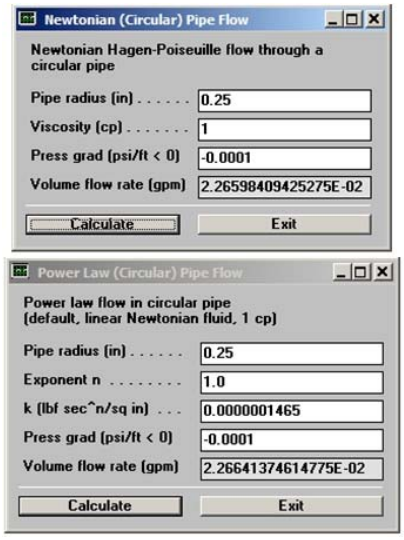

Figure 10-8a. Exact analytical solution results.

We now turn to curvilinear grid solutions which, again, do not assume axisymmetry. The Newtonian choice in Figure 10-8b invokes the three supporting menus at the left. Clicking "Simulate" leads rapidly to results shown beneath Figure 10-8b in `Courier New` font. "Iterating . . ." refers to relaxation solutions of the curved grid difference equations.

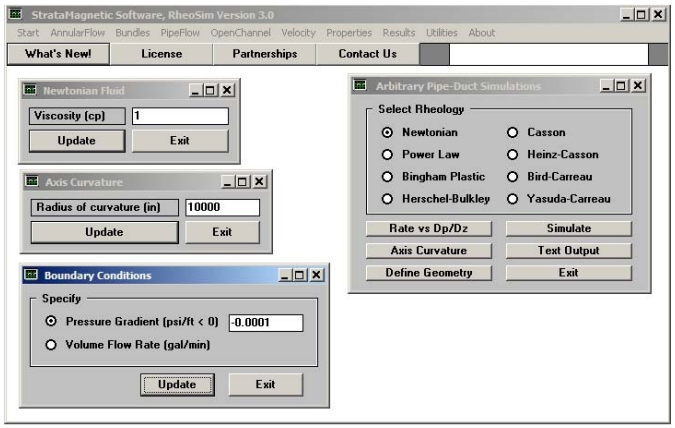

Figure 10-8b. Using PipeFlow options in curvilinear grid non-Newtonian flow simulator.

```
Iterating, please wait ...

Iteration 100, Tolerance = .9233E-03
Iteration 200, Tolerance = .2057E-04
Iteration 300, Tolerance = .5139E-06
Iteration 400, Tolerance = .0000E+00
Iteration 500, Tolerance = .0000E+00

Total, volume flow rate:  .2263E-01 gal /min
Cross - sectional  area:  .1961E+00 sqr inch
Kinetic energy, density:  .2541E-01 in^4/s^2

Area weighted means for absolute value taken
over entire pipe (x,y) cross-sectional area

O  Axial flow velocity  (inches / sec):  .3937E+00
O  Apparent viscosity (lbf sec / sqin):  .1465E-06
O  Viscous stress AppVis x dU/dx (psi):  .4289E-06
O  Viscous stress AppVis x dU/dy (psi):  .5128E-06
O  Dissipation fnctn (lbf/(sec sq in)):  .4199E-05
O  Shear rate dU/dx (Recip sec, 1/sec):  .2927E+01
O  Shear rate dU/dy (Recip sec, 1/sec):  .3500E+01
O  Stokes product Vel x ApVis (lbf/in):  .5768E-07
```

Figure 10-8c. Curvilinear grid finite difference results.

Note that the exact "πR^2"cross-sectional area should be 3.14159 (0.25) (0.25) or 0.1963 in^2. Our numerical solution, obtained on a relatively coarse mesh, yields 0.1961 in^2 which provides an important check point The exact volume flow rate found previously was 0.02266 gpm whereas the solution here is 0.02265 gpm, for a very small 0.1% error. These results establish a measure of baseline credibility.

Simulation No. 2 – Power Law flow in a perfect circle.

Next we consider the same problem for a perfect circle but assuming Power Law properties. The assumptions are shown in Figure 10-9a. Note that we have assumed n = 0.7 and K = 0.00001465 lbf sec^n/in^2 which, if this flow were Newtonian, would represent ten times the viscosity of water. In Simulation No. 1, we specified pressure gradient, but here we are prescribing a more complicated volume flow rate instead.

Thus, there are two levels of iteration. First, a test pressure gradient is assumed for the initial calculation, and iterations solving the curved grid equations are solved until convergence. If the final result does not agree with the prescribe flow rate, a "half-step method" correction is used. The Windows solution requires about 5 seconds of desk time.

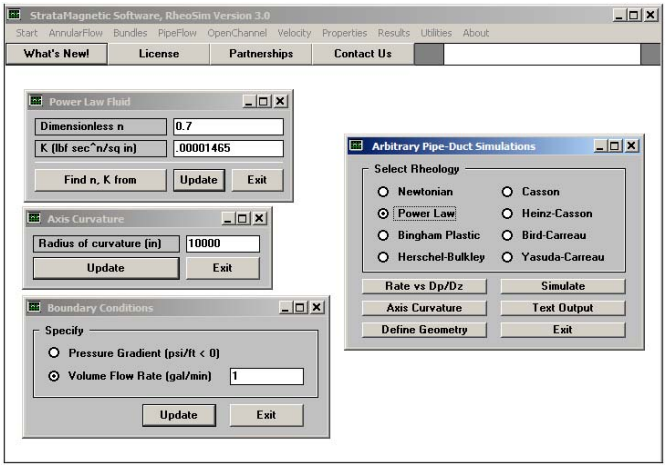

Figure 10-9a. Power Law run with flow rate specified – note, a 1 gpm target volume flow rate is about 63 ml/s.

```
O  Axial pressure gradient of .8906E-01 psi/ft
   yields volume flow rate of .1006E+01 gal/min.
   Iterations continuing ...

Pressure gradient found iteratively, .8906E-01 psi/ft,
yielding .1006E+01 gal/min vs target .1000E+01 gal/min.

Total, volume flow rate:  .1006E+01 gal /min
Cross - sectional  area:  .1961E+00 sqr inch
Kinetic energy, density:  .4968E+02 in^4/s^2

Area weighted means for absolute value taken
over entire pipe (x,y) cross-sectional area

O  Axial flow velocity  (inches / sec):  .1753E+02
O  Apparent viscosity (lbf sec / sqin):  .3171E-05
O  Viscous stress AppVis x dU/dx (psi):  .3636E-03
O  Viscous stress AppVis x dU/dy (psi):  .4347E-03
O  Dissipation fnctn (lbf/(sec sq in)):  .1569E+00
O  Shear rate dU/dx (Recip sec, 1/sec):  .1296E+03
O  Shear rate dU/dy (Recip sec, 1/sec):  .1540E+03
O  Stokes product Vel x ApVis (lbf/in):  .6427E-04
```

Figure 10-9b. Curved grid Power Law solution for circle.

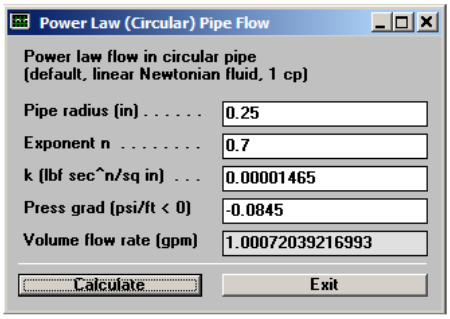

Figure 10-9c. Exact Power Law solution for circular pipe.

But just how accurate is the curved grid finite difference solution in Figure 10-9b? The results show that, for our target flow rate of 1 gpm, the required pressure gradient is 0.08906 psi/ft. In Figure 10-9c, the exact analytical solution shows that 1 gpm is achieved with a pressure gradient of 0.0845 psi/ft. Thus, the error is a small 5% where, we accentuate, we have not "fine tuned" the mesh to improve the solution.

Simulation No. 3 – Power Law flow results in a clogged conduit.

Now, we use exactly the same menu assumptions as in Figure 10-9a above, except that the circular geometry is changed to one that is clogged. The main results are shown in Figure 10-10a. Note that the pressure gradient (magnitude) is 0.1500 psi/ft and is much greater than the 0.08906 psi/ft in Simulation No. 2 due to the fact that a smaller area is used to pass the same flow rate. In Figure 10-10b, for the axial velocity field, the clog is displayed as the result of a straight vertical cut – actually, any arbitrary geometric deformation is permitted. The shear rates $\partial u/\partial x$ and $\partial u/\partial y$ are shown in Figure 10-10c, while the viscous shear stresses $\eta(x,y)\ \partial u/\partial x$ and $\eta(x,y)\ \partial u/\partial y$ are shown in Figure 10-10d. Here, $\eta(x,y)$ is the apparent viscosity in Figure 10-10e, which is also determined as part of the iterative solution. Unlike the Newtonian viscosity, the apparent viscosity depends on the flow rate or pressure gradient, plus the geometric details of the cross-section *and* the location of the point in question. Net shear rates and shear stresses are no longer axisymmetric as with circular cross-sections. Observe that while our grid is boundary-conforming, we have made no attempt to distribute perimeter points uniformly. In a practical engineering calculation where matches with data are needed, this would represent an additional step in the workflow.

```
O  Axial pressure gradient of .1500E+00 psi/ft
   yields volume flow rate of .1010E+01 gal/min.
   Iterations continuing ...

Pressure gradient found iteratively, .1500E+00
psi/ft,
yielding .1010E+01 gal/min vs target .1000E+01
gal/min.

Total, volume flow rate:  .1010E+01 gal /min
Cross - sectional  area:  .1484E+00 sqr inch
Kinetic energy, density:  .6617E+02 in^4/s^2

Area weighted means for absolute value taken
over entire pipe (x,y) cross-sectional area

O  Axial flow velocity  (inches / sec):  .2391E+02
O  Apparent viscosity (lbf sec / sqin):  .2696E-05
O  Viscous stress AppVis x dU/dx (psi):  .3379E-03
O  Viscous stress AppVis x dU/dy (psi):  .7140E-03
O  Dissipation fnctn (lbf/(sec sq in)):  .3709E+00
O  Shear rate dU/dx (Recip sec, 1/sec):  .1329E+03
O  Shear rate dU/dy (Recip sec, 1/sec):  .2986E+03
O  Stokes product Vel x ApVis (lbf/in):  .7248E-04
```

Figure 10-10a. Power Law flow in clogged blood vessel.

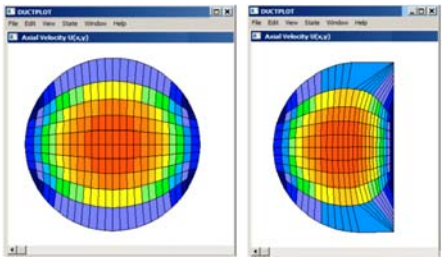

Figure 10-10b. Velocity solutions for unclogged circular section (left) and clogged section (right) for Power Law flow. Clog is displayed as result of vertical cut. Colored regions are flow areas (red is high). The same color represents different values as they were obtained in two different simulations.

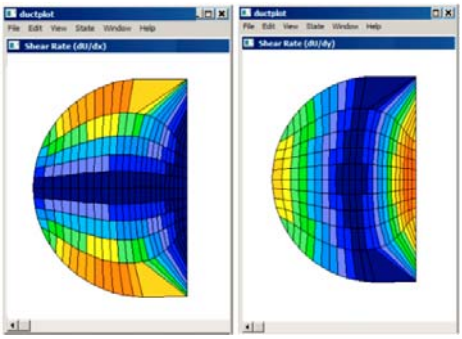

Figure 10-10c. Shear rates in Power Law flow.

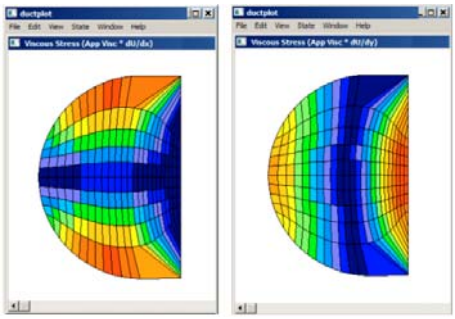

Figure 10-10d. Viscous shear stress in Power Law flow.

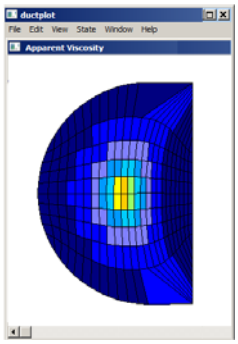

Figure 10-10e. Apparent viscosity η(x,y) in Power Law flow.

Conclusions

We successfully performed several tasks in our research on non-Newtonian flow in clogged non-circular pipes:

1. A fast finite difference algorithm for arbitrary duct geometries hosted by boundary-conforming curvilinear grids was developed;
2. The method provides high-resolution solutions for axial velocity, apparent viscosity, and x and y shear rates and viscous shear stresses everywhere;
3. Stresses can be used to determine the ability of a duct to self-clean in the presence of debris-building mechanisms;
4. Nonlinear pressure drop versus volume flow rate relationships can be calculated by performing the calculation for different pressure drops and used in pump power, pipeline cleaning and economic applications.

About the Author

Jamie is a Program Analyst with Stratamagnetic Software, LLC in Oklahoma City. In addition to pipe flow and petroleum engineering applications, she is interested in biological fluid mechanics and has developed specialized models for arteries, capillaries and veins. Jamie is co-author of the monograph *Biofluids Modeling – Methods, Perspectives and Solutions*, forthcoming from scientific book publisher John Wiley & Sons in 2022. For more software or company contact information, please visit www.stratamagnetic.com.

Acknowledgments

This research is an outgrowth of 2009-2011 work supported by the United States Department of Energy for "Advanced Steady-State and Transient, Three-Dimensional, Single and Multiphase, Non-Newtonian Simulation System for Managed Pressure Drilling." That investigation was administered by RPSEA Subcontract No. 08121-2502-01. The original grid generation work was supported by US DOE Small Business Innovation Research Grant DE-FG03-99ER82895 in 1999-2000. The author also acknowledges W.C. Chin for suggesting and guiding the present effort.

References

1. Becker, T.E., Azar, J.J., and Okrajni, S.S. 1989. "Correlations of Mud Rheological Properties with Cuttings Transport Performance in Directional Drilling." SPE Paper No. 19535, *64th Annual Technical Conference and Exhibition*, Society of Petroleum Engineers, San Antonio, October 1989.
2. Chin, W.C. 2012. *Managed Pressure Drilling: Modeling, Strategy and Planning,* Elsevier Scientific Publishing, Amsterdam.
3. Thompson, J.F. 1984, "Grid Generation Techniques in Computational Fluid Dynamics." *AIAA Journal*, November 1984, pp. 1505-1523.
4. Thompson, J.F., Warsi, Z.U.A. and Mastin, C.W. 1985. *Numerical Grid Generation*, Elsevier Science Publishing, New York, 1985.